Applied Materials Today 6 (2017) 16–21

Contents lists available at ScienceDirect

Applied Materials Today

journal homepage: www.elsevier.com/locate/apmt

High-performance ink-jet printed graphene resistors formed with environmentally-friendly surfactant-free inks for extreme thermal environments

Monica Michel [a], Chandan Biswas [b], Anupama B. Kaul [b,*]

[a] Metallurgical, Materials and Biomedical Engineering, University of Texas at El Paso, El Paso, TX 79968, United States
[b] Electrical and Computer Engineering, University of Texas at El Paso, El Paso, TX 79968, United States

ARTICLE INFO

Article history:
Received 3 November 2016
Received in revised form 4 December 2016
Accepted 5 December 2016

Keywords:
Ink-jet printing
Graphene
Environmentally-friendly inks
Chemical-exfoliation
Surfactants

ABSTRACT

In this work, a surfactant-free graphene ink is prepared in a mixture of terpineol (*T*) and cyclohexanone (*C*) and optimized to yield rheologies appropriate for ink-jet printing on both rigid SiO_2/Si and flexible polyimide substrates. The surfactant-free ink optimized here, clearly demonstrates its enhanced electrical transport characteristics, where resistivity ρ values are 7× lower, i.e. 1.1 mΩ m, compared to 7.1 mΩ m for the surfactant-assisted formulations derived from N-methyl-2-pyrrolidone (NMP) and ethyl cellulose (EC) reported earlier. The *C:T* surfactant-free ink is stable with aging, exhibiting minimal signs of graphene nano-membrane re-agglomeration. The mechanical elasticity and robustness of the printed structures is evaluated through strain-dependent bending tests that reveal minimal variations in resistance (~8%) with bending radii of curvature up to 0.16 cm^{-1}. Finally, the thermal behavior of the printed features formed using the surfactant-free ink is deciphered from the Resistance–Temperature data obtained from 6 K to 350 K, where the temperature coefficient of resistivity (TCR) is calculated to be very low (e.g. 1 Ω/K in the range of 6–80 K, or -2.7×10^{-4} ppm/K), comparable to other low TCR materials such as polymer/carbon composites. In summary, the resistive structures designed using the surfactant-free, environmentally-friendly inks formulated here, exhibit attributes that are extremely desirable for flexible electronics, such as enhanced electronic transport, good mechanical robustness and a TCR that varies minimally with temperature.

1. Introduction

The unique mechanical, thermal and electrical properties of two-dimensional (2D) layered materials (LMs) [1–3] have come into prominence in recent years with our ability to isolate single layers from a wide variety of 2DLMs, such as hexa-boron nitride (h-BN), transition metal dichalcogenides, metal halides, and carbo-nitrides [4,5]. One approach that is used to obtain dispersions of these 2D crystals, that is attractive from a large-area manufacturing stand point, is liquid-phase exfoliation (LPE) [6,7]. These solution-processing approaches obviate the need for expensive cleanrooms with complex lithography steps that often utilize toxic compounds. Solution-based approaches lend themselves toward the exploration of simple, cheap and additive manufacturing techniques that are compatible with large-area production. In these methods, layers of the 2D materials are deposited through various fabrication techniques [8–10], such as drop and spray coating, roll-to-roll transfer, doctor blading, gravure printing, as well as ink-jet printing [11,12], which is a technique we have focused on in this work.

Ink-jet printing is poised to impact the manufacturing of devices that are particularly attractive for flexible electronics, as more suitable and printable fluids become available. The addition of surfactants in the preparation of the inks usually results in additional process steps, potentially increasing cost, as well as material waste, where the surfactants also often have a negative impact on specific properties of the printed features, such as comprising electrical conductivity of metallic structures. The first step in the preparation of an ink is the successful exfoliation of the bulk material using chemical solvents [13,14]. The most promising solvents for exfoliating and achieving stable suspensions of 2DLMs, in particular graphene, have been reported to be N-methyl-2-pyrrolidone (NMP), *N,N*-dimethylacetamide (DMA) and dimethylformamide (DMF) [6]. Another option is to use a solvent exchange process which has already proven to be successful with ethanol and terpineol [15,16]. In many cases, the solvents commonly used are toxic, and so there is an impetus for producing more environmentally friendly options of solution dispersions for sustainability [17]. In this work, we have successfully formulated a suitable ink derived

* Corresponding author.
E-mail address: akaul@utep.edu (A.B. Kaul).

http://dx.doi.org/10.1016/j.apmt.2016.12.001
2352-9407/

from a mixture of terpineol (*T*) in cyclohexanone (*C*) as a more environmentally friendly option for the exfoliation of bulk graphite, which we elaborate upon in more detail here.

Despite the fact that the 2DLMs may be exfoliated successfully into few-layer nanomembranes, the specific rheological characteristics of the dispersion needs to be optimized to make it suitable for ink-jet printing; eventually parameters such as viscosity, surface energy and density play a domineering role in determining whether or not the dispersion can be successfully implemented for ink-jet printing [18]. Surfactants have long been used to modify the surface energy and viscosity of dispersions and some prior studies include material systems of pyrene carboxylic acid, sodium dodecylbenzene sulfonate (SDBS), amphiphilic copolymers, and ethyl cellulose (EC) [19,20]. Often times, the surfactants used in the formulations are intentionally removed in order to avoid detrimental consequences that compromise properties of the printed features such as electrical conductivity. In other cases, functionalized graphene is used and results in graphene oxide (GO) which later is converted to reduced graphene oxide (RGO) [21–23]; while the effect of oxides can be negated through the reduction stage, it nonetheless adds yet another processing step, not to mention the additional defects that are formed.

The motivation for this work is to develop a solution dispersion that does not rely on the addition of any surfactant, functionalization group or stabilizer to begin with, and yet it possesses the rheological properties that make it suitable for ink-jet printing. We have succeeded in creating such a dispersion, where the viscosity values of *T* and *C* are optimized to yield a printable ink, but where the exfoliating potential of *T* is also noted. Surfactant is used to aid in the stability of the dispersions which has been necessary in prior reports on the ink-jet printing of 2DLMs to avoid agglomeration that leads to nozzle clogging over time. Remarkably, our prepared inks are stable for weeks without the need for surfactants, where a brief sonication step for a few minutes is necessary to condition the dispersion just prior to ink-jet printing. Our nozzles remained clear and clog-free for weeks after the initial ink filling.

After formulating the inks, as noted above, we have studied the properties of the printed features to understand the role of annealing on the transport characteristics of the printed inks. This ink was used to print resistive device structures on both rigid SiO_2/Si and flexible polyimide substrates. Strain-dependent bending tests revealed that our printed features exhibited minimal change in electrical transport properties with strain, indicating intrinsic robustness of the graphene nanomembranes themselves, as well as good adherence of the printed features to the flexible polyimide substrates. The thermal stability of the printed features was also evaluated, where the change in resistance was measured as a function of temperature in the 6–350 K range. When temperature varies, most materials show a temperature dependent resistance change, as denoted by the temperature coefficient of resistance (TCR), where TCR can be positive if the resistance increases as temperature increases, and negative for the converse case. Additionally, for some applications a large TCR is desirable, such as thermistors and temperature sensors, where a small change in temperature should yield a large change in the resistivity for such devices to operate ideally. In other situations, a temperature independent TCR is needed, which are referred to as near-zero-(NZ)-TCR materials. Such materials are created intentionally to display this NZ-TCR characteristic; for example, bi-layer composites, comprising of polymers with a carbon nanotube base (having negative TCR) and a carbon black base (having positive TCR), yield a hybrid structure where resistance changes minimally with temperature with small TCR ~ 2% [24]. In this work, the smallest variation from the normalized resistance was also found to be less than 2% with a negative TCR throughout the entire 6–350 K range. In other material systems such as antiperovskites, an anomalous change in electronic transport from the metallic behavior is seen at 200 K where the NZ-TCR regime is noted due to correlated ionic moments aligning below 200 K [25]. Other inorganic composites with low or NZ-TCR behavior comprise of fine TaN/Cu particles in the tens of nm range, where the TCR value can be tuned by varying the TaN/Cu ratio [26]. We believe our work is the first report of a 2DLM based ink-jet printed device that exhibits a low TCR where resistance changes minimally with temperature. Thus, our surfactant-free dispersions yield not only printable and stable inks, but the resistive device structures formed with these inks display very low TCR values, and exhibit an electrical response that was immune to bending or mechanical strain, making them highly attractive for printed and flexible electronics.

2. Materials and methods

The solvents used in this work, terpineol (*T*) and cyclohexanone (*C*) were purchased from Sigma-Aldrich and used as received to prepare ink mixtures at different ratios. The viscosity measurements were conducted using a Brookfield DV-E viscometer. The graphite rod (GR) (Sigma–Aldrich #496553) was dispersed in the different solvent mixtures at a concentration of 10 mg/ml, and placed in a bath sonicator for 24 h. Supernatants from the dispersions were used for the optical absorption measurements. *Printing.* The DIMATIX 2831 material printer from Fujifilm was used for the ink-jet printing, where the ink cartridges were purchased from the manufacturer and had a volume of 10 pl, with 16 nozzles and a nozzle diameter of ~21.5 μm. *Characterization:* SEM microscopy was carried out in a Hitachi S-4800. Electrical characterization was conducted using a micromanipulator 450PM-B probe stage equipped with an HP precision semiconductor parameter analyzer 4156A. A Lakeshore CRX-4K probe station was used to obtain the resistance as a function of temperature with a Keysight B1500-A Semiconductor Device Analyzer. Profilometer measurements were performed on the Brocker Dektak XT Stylus Profiler. *Substrate:* SiO_2/Si wafers with a 300 nm oxide layer and polyimide substrates were used for ink-jet printing.

3. Results and discussion

3.1. Viscosity and absorption measurements

The solvents *T* and *C* have been previously studied as dispersants for graphene by various groups, but in these prior reports the addition of a surfactant was also included in the formulations [27,28]. Due to its higher viscosity, *T* can be used to tune the viscosity of the ink to achieve the recommended 10 cP for optimal printing. Various ratios of *T* in *C* were prepared and their viscosity was measured in order to find the optimum viscosity for ink-jet printing. Fig. 1a shows the change in viscosity values for the *C:T* mixture; for example, with 0% *T*, or 100 % *C*, a viscosity of 2 cP resulted, while 100% *T* exhibited a viscosity ~39 cP. The optimum viscosity was achieved at 80%*T* with a value of 10 cP. The secondary horizontal axis (on top) of Fig. 1a shows the results of previously reported work in which the viscosity of a *C:T* mixture at a ratio of 7:3 solution in NMP was modified with the addition of EC [20,29]; we refer to this as the surfactant-assisted formulation for comparative purposes. The area of the optimum viscosity for printing is indicated by the blue shaded region in Fig. 1a.

The GR ink was prepared with different ratios of the in *C:T* using a procedure denoted in the methods section, and the dispersions were allowed to stabilize overnight where the supernatant was used for characterization and printing optimization. Optical absorbance spectroscopy was used to analyze the dispersions and the results obtained are shown in Fig. 1b. Absorbance

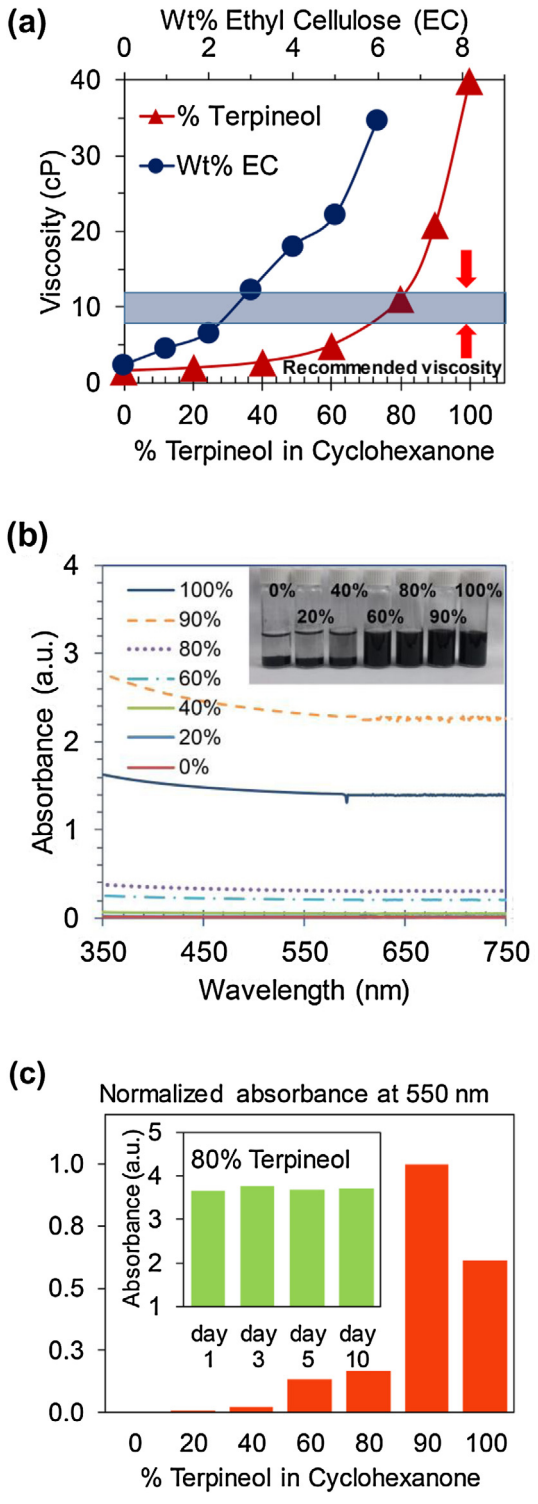

Fig. 1. (a) Change in viscosity values for different solvents. Primary horizontal axis showing % of terpineol in cyclohexanone (*C/T*) and secondary horizontal axis showing *T*/*C* (7:3) in NMP with increasing wt% of EC. (b) Absorbance values obtained for the graphite rod (GR) dispersed in increasing percentage ratios of *T*in*C*. Insets showing vials of the GR dispersions in increasing percentage ratios of *T*in*C*. (c) Normalized absorbance values at a wavelength of 550 nm of the GR dispersed in various percentages of C/T*C*/*T*; inset shows the absorbance values for the prepared GR dispersions in 80% *T*taken as a function of time, indicating the dispersions to be stable with aging.

measurements revealed that as the concentration of *T* in the dispersion was increased, the absorption increased, where the highest absorbance was seen to occur at $T \sim 90\%$. This data clearly suggests that *T* has an important role to play in effectively exfoliating the graphite into nanomembranes, which is also corroborated by the optical images of the vials in the inset of Fig. 1b, where the dispersions look darker in color as the % *T* increases. The enhanced exfoliation of graphite in *T* was further highlighted in Fig. 1c, which depicts the normalized absorbance values at a wavelength of 550 nm, and the increase in the absorbance as *T* increased is clearly evident, where a maximum is noted to occur at 90% *T*. However, we proceed with the ink formulation for $T \sim 80\%$, given the fact that the viscosity for the 90% case was ~20 cP that fell well outside the optimal regime of 8–12 cP for viscosity suitable for ink-jet printing. The stability of the dispersions with time was evaluated and the data are shown in the inset of Fig. 1c, which illustrates the absorbance was unchanging with time over the course of 10 days.

3.2. Electrical characterization measurements

After optimizing the rheological properties of our ink formulations, we began to explore the electronic transport characteristics of the dispersions once they were drop cast onto SiO_2/Si substrates and annealed for 1 h at 350 °C, prior to conducting the current–voltage (*I–V*) measurements. Current–voltage measurements were obtained for the graphene ink prepared at different ratios of *C:T*, and the results are shown in Fig. 2a. The graphite dispersed in 100% *T* showed the highest current values (1 mA at 1 V) with the current decreasing with reduced *T* concentration. Fig. 2b demonstrates the resistance values generally decreasing as the % *T* increases in *C*. The insets in Fig. 2b show the microstructures of our drop cast samples that were obtained using scanning electron microscopy (SEM). The 0% *T* dispersion shown at the top (100% *C*) displays nearly bulk platelets that exhibit voids and poor spatial uniformity. For the 80% *T* case however (SEM shown in bottom inset), the exfoliated material formed a conductive film comprised of thinner and more uniform flakes which is consistent with the higher conductance values seen in this case. It was apparent from the structural characterization, as well as the electronic transport data, that a concentration of 80% *T* provided optimal exfoliation of the graphite.

Our ink-jet printed surfactant-free ink was further characterized using Raman spectroscopy, which is a non-invasive technique used to characterize the structural and electronic properties of materials. The Raman shift is depicted in Fig. 2c, which shows the well-defined D band (1350 cm^{-1}), G band (1580 cm^{-1}) and a 2D or G′ band (2700 cm^{-1}), indicating the presence of multi-layer graphene.

Fig. 3a shows *I–V* curves comparing the drop casted surfactant-free 80% *T* graphene ink (left vertical axis) and the surfactant-assisted graphene ink (right vertical axis); here the surfactant-assisted ink comprises of EC and NMP, as noted earlier. Surfactant-free ink resulted in two orders of magnitude greater current values (5 mA at 1 V of applied voltage, or a resistance value ~189 Ω) compared to the surfactant-assisted ink (0.06 mA at 1 V, or a resistance value ~18 kΩ). Fig. 3b and c shows SEM micrographs of the surfactant-free and surfactant-assisted film, respectively, resulting from GR inks. An inference of an approximate platelet size can be made from Fig. 2b, and Fig. 3b and c, where the SEM images can shed some insights on their size. From Fig. 2b upper inset, the platelet size can be approximated to be 5–10 μm, while from Fig. 2b bottom inset, the size appears to be substantially lower, well below 5 μm in the case of the 80% *T*. The higher resolution SEM images in Fig. 3b and c show the size to be clearly below 5 μm, approximately in the range of 1 μm or less. Both resulting films show large-area uniformity with approximately a similar platelet size; however, the continuous presence of the surfactant affects

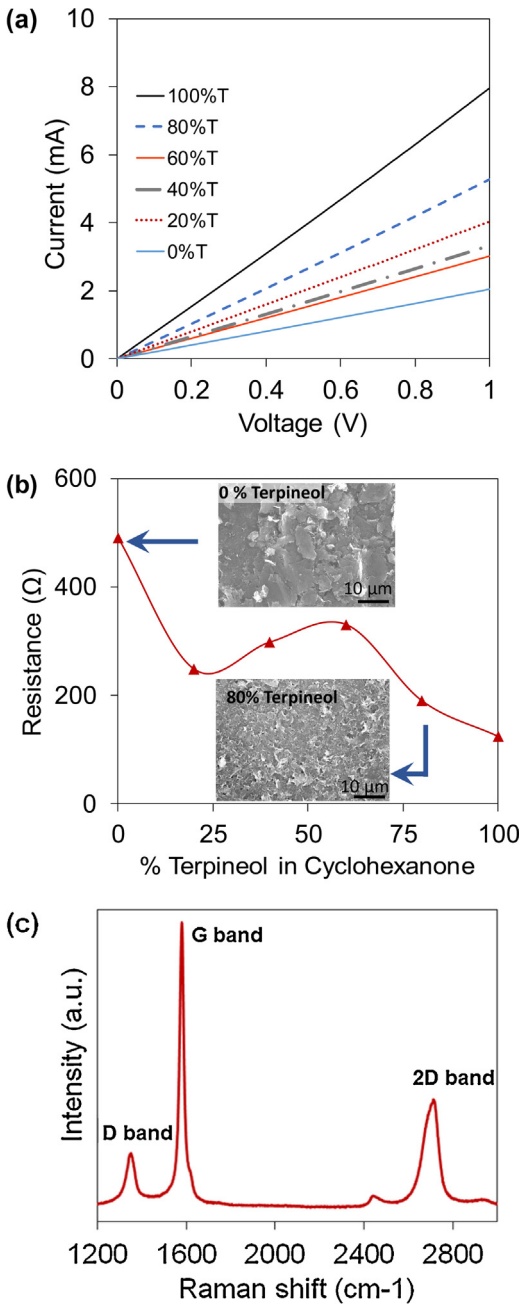

Fig. 2. (a) *I–V* measurements of the GR dispersed in different ratios of *C/T* that were drop casted onto SiO_2/Si substrate and annealed for 1 h at 350 °C. (b) Resistance values obtained from the dispersions with different ratios of *C/T*. Insets of SEM micrographs of the surface morphology for dispersions made with 0% *T* or 100% *C* (top) and 80% T (bottom). (c) Raman spectra obtained from printed surfactant-free ink, showing the D, G and 2D (or G′) peaks.

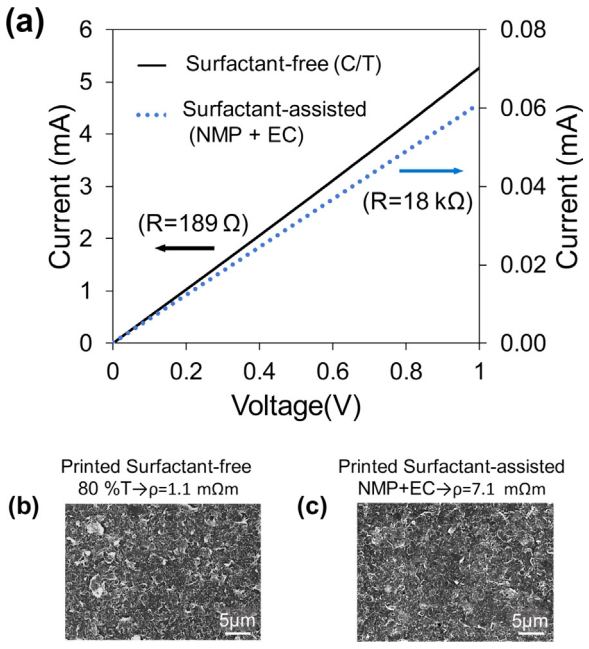

Fig. 3. (a) *I–V* measurements resulting from the drop casted GR dispersion prepared with surfactant-free 80% *C:T*(80 *T*) (primary vertical axis) and the surfactant-assisted GR dispersion (secondary vertical axis). SEM micrographs showing the resulting films after printing on SiO_2/Si substrate with (b) surfactant-free and (c) surfactant-assisted GR dispersions where ρ is 7× lower for the surfactant-free case.

the resistivity ρ by remaining embedded within the material, since $\rho \sim 7\,m\Omega\,m$ and $1.13\,m\Omega\,m$, for the surfactant-assisted ink and surfactant-free inks, respectively. Conductivity of 1.1 S/m (one fifth that of typical graphene film) has been reported and attributed to the decreased percolation of graphene plates in ink-jet printing [30]. This conductivity corresponds to a resistivity $\rho \sim 909\,m\Omega\,m$ which is much higher than the surfactant-free ink reported in this work with a value for $\rho \sim 1.1\,m\Omega\,m$. Ethyl cellulose is a polymer that possesses excellent membrane-forming ability and durability and is commonly used for flexible coatings for paper, cloth and leather. Ethyl cellulose's thermoplastic characteristics and insulating properties have been studied mostly below 200 °C, which is when decomposition is initiated [31]. Recent studies using thermogravimetric analysis (TGA) show two stages of the thermal degradation reaction for EC in the 180–300 °C region and at 370 °C. Even at higher temperatures, degradation of EC occurs slowly, and at 1000 °C about 2% remains as residual mass [32]. It is no surprise that some EC will remain in the surfactant-assisted inks even after annealing [33], which is likely to compromise the formation of an intimate contact between respective graphene nanomembranes, reducing the overall electrical conductivity of the printed film. On the other hand, in the terpineol-based surfactant-free ink, the *T* has a lower boiling point ~ 215 °C, and since our annealing temperatures are well above this, the prospect for residuals remaining is minimized, and the ensuing electrical conductivity is higher, as we observe here.

Fig. 4a demonstrates the effect of the annealing temperature on the resistance of the prepared inks, once it was ink-jet printed onto the SiO_2/Si substrate, as shown by the image of the printed structure in the inset of Fig. 4a. The printed graphene patterns were annealed for either 1 h or 2 h, and the annealing temperature was varied from 200 °C to 400 °C; the resistance values are shown in Fig. 4a as a function of the annealing temperature (vertical axis is logarithmic scale) for the two annealing times considered. Annealed samples at 200 °C and 250 °C showed very high resistance (10 MΩ and 100 MΩ). The resistance values were significantly reduced to the 300 kΩ range, when annealing temperatures were >300 °C. For annealing temperatures >300 °C, the resistance remained in the kΩ range for all annealing durations and temperatures tested, demonstrating that the minimum annealing temperature should be ~300 °C to achieve low resistance printed films.

The surfactant-free ink was used to print a pattern on SiO_2/Si and polyimide substrates at identical conditions (30 printing passes and annealed for 1 h at 350 °C). Figure 4b demonstrates the scaling of the resistance of the printed patterns as the separation between the probe tips increases. The inset of Fig. 4b shows an optical image of the printed graphite film on the polyimide substrate. The printed film on polyimide shows lower linear sheet resistance values (1.4 kΩ/mm) compared to the one printed on the SiO_2/Si substrate (2.1 kΩ/mm) substrate which may have to do with the

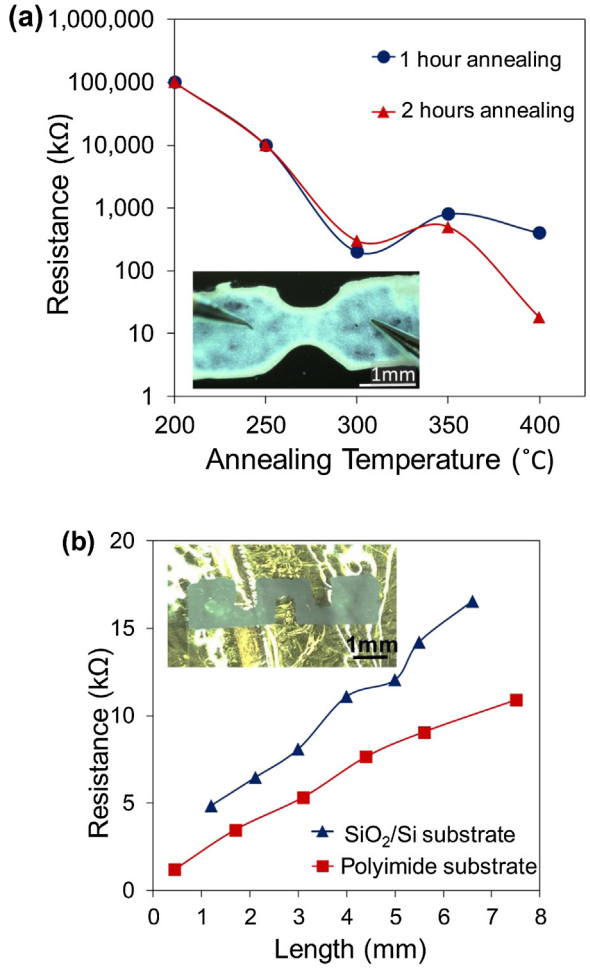

Fig. 4. (a) Variation of resistance with different annealing temperatures for 1 and 2 h. Inset showing optical image of the printed structure on SiO_2/Si. (b) Change in resistance values with respect to the probe placement distance, of printed surfactant-free ink on SiO_2/Si and polyimide substrates. Inset is optical image of printed ink on polyimide substrate.

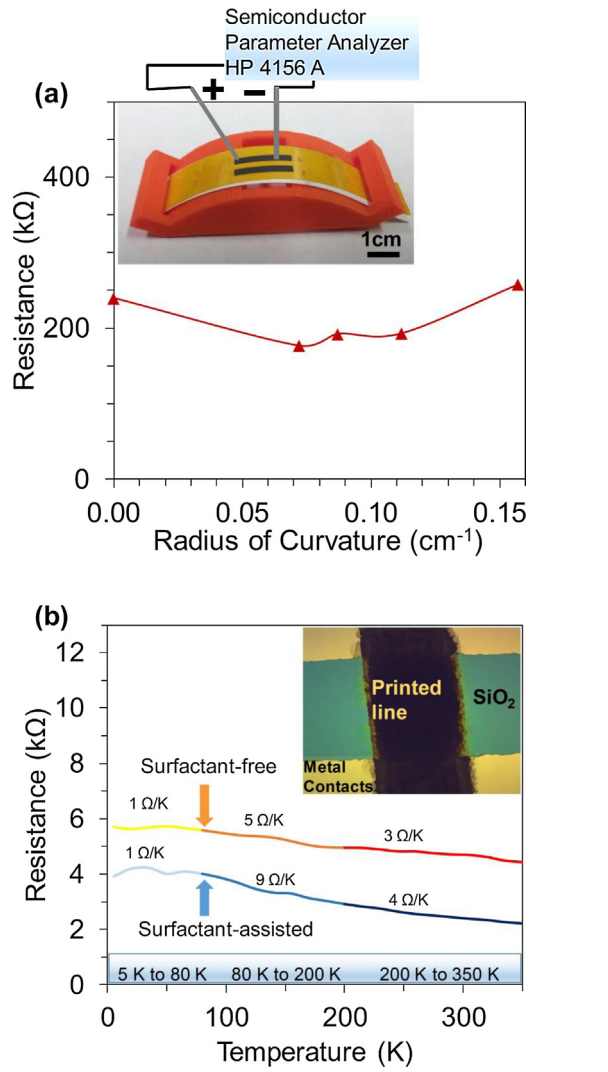

Fig. 5. (a) Resistance values changing with varying curvature radius. Inset showing schematic of the test fixture used for the strain-induced bending test. (b) Resistance values of surfactant-free and surfactant-assisted ink printed on SiO_2/Si when subjected to different temperatures from 6 K to 350 K. Indicated are the three different temperature regimes and their respective average TCR denoted as Ω/K. Inset is an optical image of the ink-jet printed line connecting the Mo contacts on the SiO_2/Si substrate for which *R–T* data was obtained.

better substrate–thin film interaction and lower thermal mismatch of the polyimide substrate compared to the SiO_2/Si substrate after heat treatment [8]. Our surfactant-free inks were thus shown to be successfully ink-jet printed onto both rigid and flexible substrates.

3.3. *Bending test*

We proceeded to gauge the mechanical robustness of the printed structures which is important for flexible electronics. For flexible electronics applications, it is expected that the printed features will experience mechanical strain given the flexible, conformable nature of the substrates. Thus, it is important to validate the effect of mechanical strain on the electronic transport properties of the devices fabricated from the inks. In order to conduct this study, line patterns were printed on flexible polyimide substrates and then placed on substrate holders with a fixed radius of curvature and the data are shown in Fig. 5a. The test was performed by keeping the distance between the probe tips constant at ~10 mm. The samples were tested at four radii of curvature, and the fixture for one such curvature is depicted in the inset of Fig. 5a. Initially, there was a slight decrease in resistance during the first two bending positions, which was followed by an increase in resistance. As bending strain was induced, the graphene nanomembranes are likely to be initially compressed at the substrate-film interface, which decreases the membrane-to-membrane separation distance and hence enhances mechanical contact and the ensuing electrical transport. With increased bending however, the current decreases as the membranes start to separate with larger bending angles, and the larger inter-membrane separation leads to a reduction in the electrical transport. The resistance values obtained as the bending test was performed still resulted in a very small increase in resistance values from 239 kΩ (no bending case) to 257 kΩ (radius of curvature ~0.157 cm^{-1}), which accounts for a total change in resistance of less than 8%. Other conductive materials have previously been used for flexible substrates, such as one-dimensional (1D) silver nanowires or copper; however, they are more expensive, and due to the high aspect ratio of nanowires (i.e. diameter of 55 nm, length of 8.1 μm), it is extremely difficult to print such structures without blocking the nozzles. In addition, the density of these wires deposited per volume of liquid printed is low, making them impractical for printing [34]. The ink formulation prepared in this work utilizes very cheap, earth-abundant graphite where the 2D layered morphology is beneficial to ensuring larger contact area between nanomembranes that is also advantageous for mechanical resilience, compared to a network of 1D conductors.

3.4. Resistance versus temperature measurements

In order to evaluate the thermal stability of the surfactant-free inks, the resistance R versus temperature T characteristic was measured from 6 K to 350 K, as shown in Fig. 5b, using a cryogenic probe stage that was equipped with a closed cycle refrigerator. Metal contacts (molybdenum) were deposited on SiO_2/Si substrates and graphene-based inks were then printed in between the Mo electrodes, as shown in the inset of Fig. 5b. As shown by the data in Fig. 5b, the R–T characteristic for both the surfactant-free and the surfactant-assisted ink is shown for comparative analysis. Both inks displayed a negative temperature coefficient of resistance (TCR), where the R decreases with increasing T. In addition, on average, the surfactant-free ink demonstrates a lower TCR over the entire thermal range compared to the surfactant-assisted ink, with TCR calculated from 5 to 80 K, 80 to 200 K, and 200 to 350 K to be $\sim -2.77 \times 10^{-4}$, -9.4×10^{-4}, and -7×10^{-4} ppm/K (1, 5 and 3 Ω/K), respectively. The variation of the surfactant-free ink with the increase in temperature can be calculated over the entire temperature range of 344 K (i.e. from 6 K to 350 K) to be ~3%. In contrast, the surfactant-assisted ink had higher TCR values in the three regimes of $\sim 3.1 \times 10^{-4}$, -2.3×10^{-4}, and -1.6×10^{-4} ppm/K, (1, 9 and 4 Ω/K) respectively. In other reported materials, the range of temperatures studied is smaller (180 K [24]) with a variation in resistance of 2%. Therefore, the printed graphite film formed using a surfactant-free ink demonstrated minimal variation with temperature, which is attractive for applications where constant values of resistance over a wide range of temperatures maybe desirable for flexible electronics applications.

4. Conclusions

A surfactant-free graphene ink was prepared with the use of environmentally friendly terpineol and cyclohexanone and the ratio of the mixture was optimized to obtain the characteristics required for good drop formation, jetting and ink-jet printing. The prepared ink showed good stability that only requires mild sonication before its use to avoid agglomeration. The optimum post printing temperature and duration of annealing were found to be 350 °C for 1 h, which resulted in uniform film formation and a ρ that was 7× lower compared to the surfactant-assisted NMP-EC based formulation. The surfactant-free ink was successfully printed on both rigid SiO_2/Si and flexible polyimide substrates. Minimal change in resistance was observed with strain-induced bending, suggesting good adhesion characteristics between the substrate and the printed ink. The resulting device demonstrated a low TCR over a wide range of temperatures, making it suitable for applications where constant resistance values are required in extreme thermal environments.

Acknowledgements

A.B.K. acknowledges the University of Texas System Faculty Science and Technology Acquisition and Retention (STARS) award (EC284802) for the acquisition of equipment in the establishment of the Nanomaterials and Devices Lab at the University of Texas, El Paso (UTEP). Support provided by the UTEP start up grant is also acknowledged for MM. We also thank the Army Research Office (ARO W911NF-15-1-0425) that enabled us to pursue this work. Additionally, we thank Dr. Deidra Hodges for the Mo-deposition, and Gustavo A. Saenz for his assistance in the R–T measurements.

References

[1] A. Geim, K. Novoselov, The rise of graphene, Nat. Mater. 6 (2007) 183.
[2] K. Novoselov, A. Geim, S. Morozov, D. Jiang, Y. Zhang, S. Dubonos, I. Grigorieva, A. Firsov, Electric field effect in atomically thin carbon films, Science 306 (2004) 666.
[3] X. Mingsheng, T. Liang, M. Shi, H. Chen, Graphene-like two-dimensional materials, Chem. Rev. 113 (2013) 3766.
[4] L. Song, Z. Liu, A.L.M. Reddy, N.T. Narayanan, J. Taha-Tijerina, J. Peng, G. Gao, J. Lou, R. Vajtai, P.M. Ajayan, Binary and ternary atomic layers built from carbon, boron, and nitrogen, Adv. Mater. 24 (2012) 4878.
[5] A.B. Kaul, Two-dimensional layered materials: structure, properties, and prospects for device applications, J. Mater. Res. 29 (2014) 348.
[6] J. Coleman, M. Lotya, A. O'Neill, S. Bergin, P. King, U. Khan, K. Young, A. Gaucher, S. De, R. Smith, Two-dimensional nanosheets produced by liquid exfoliation of layered materials, Science 331 (2011) 568.
[7] V. Valeria Nicolosi, M. Chhowalla, M.G. Kanatzidis, M.S. Strano, Liquid exfoliation of layered materials, Science 340 (2013) 1226419.
[8] W.S. Wong, A. Salleo, Flexible Electronics: Materials and Applications, Springer Science & Business Media, 2009.
[9] N. Arokia, A. Ahnood, M.T. Cole, S. Lee, Y. Suzuki, P. Hiralal, F. Bonaccorso, Flexible electronics: the next ubiquitous platform, Proc. IEEE 100 (2012) 1486.
[10] H.W. Choi, T. Zhou, M. Singh, G.E. Jabbour, Recent developments and directions in printed nanomaterials, Nanoscale 7 (2015) 3338.
[11] E.B. Secor, P.L. Prabhumirashi, K. Puntambekar, M.L. Geier, M.C. Hersam, Inkjet printing of high conductivity, flexible graphene patterns, J. Phys. Chem. Lett. 4 (2013) 1347.
[12] A. Capasso, D.R. Castillo, H. Sun, A. Ansaldo, V. Pellegrini, F. Bonaccorso, Ink-jet printing of graphene for flexible electronics: an environmentally-friendly approach, Solid State Commun. 224 (2015) 53.
[13] Y. Hernandez, V. Nicolosi, M. Lotya, F.M. Blighe, Z. Sun, S. De, I. McGovern, B. Holland, M. Byrne, Y.K. Gun'Ko, High-yield production of graphene by liquid-phase exfoliation of graphite, Nat. Nanotechnol. 3 (2008) 563.
[14] M. Lotya, Y. Hernandez, P.J. King, R.J. Smith, V. Nicolosi, Liquid phase production of graphene by exfoliation of graphite in surfactant/water solutions, J. Am. Chem. Soc. 131 (2009) 3611.
[15] X. Zhang, A.C. Coleman, N. Katsonis, W.R. Browne, B.J. Van Wees, B.L. Feringa, Dispersion of graphene in ethanol using a simple solvent exchange method, Chem. Commun. 46 (2010) 7539.
[16] J. Li, F. Ye, S. Vaziri, M. Muhammed, M.C. Lemme, M. Östling, A simple route towards high-concentration surfactant-free graphene dispersions, Carbon 50 (2012) 3113.
[17] J. Chen, B. Yao, C. Li, G. Shi, An improved hummers method for eco-friendly synthesis of graphene oxide, Carbon 64 (2013) 225.
[18] B. Derby, Inkjet printing of functional and structural materials: fluid property requirements, feature stability, and resolution, Annu. Rev. Mater. Res. 40 (2010) 395.
[19] L. Guardia, M. Fernández-Merino, J. Paredes, P. Solis-Fernandez, S. Villar-Rodil, A. Martinez-Alonso, J. Tascón, High-throughput production of pristine graphene in an aqueous dispersion assisted by non-ionic surfactants, Carbon 49 (2011) 1653.
[20] M. Michel, J.A. Desai, C. Biswas, A.B. Kaul, Engineering chemically exfoliated dispersions of two-dimensional graphite and molybdenum disulphide for ink-jet printing, Nanotechnology 27 (8) (2016), 485602.
[21] S. Park, R.S. Ruoff, Chemical methods for the production of graphenes, Nat. Nanotechnol. (2009) 217.
[22] P. Sungjin, A. Jinho, J. Inhwa, R.D. Piner, S.J. An, Colloidal suspensions of highly reduced graphene, Nano Lett. 9 (2009) 1593.
[23] D.R. Dreyer, S. Park, C.W. Bielawski, R.S. Ruoff, The chemistry of graphene oxide, Chem. Soc. Rev. 39 (2010) 228.
[24] K. Chu, S.C. Lee, S. Lee, D. Kim, C. Moon, S.H. Park, Smart conducting polymer composites having zero temperature coefficient of resistance, Nanoscale 7 (2015) 471.
[25] L. Ding, W. Cong, C. Lihua, Y. Jun, N. Yuanyuan, H. Qingzhen, C. Xiaolong, Near zero temperature coefficient of resistivity in antiperovskite $Mn_3Ni_{1-x}Cu_xN$, Appl. Phys. Lett. 99 (2011) 251905.
[26] B. Fu, L. Gao, Tantalum nitride/copper nanocomposite with zero temperature coefficient of resistance, Scr. Mater. 55 (2006) 521.
[27] Y. Gao, W. Shi, W. Wang, Y. Leng, Y. Zhao, Inkjet printing patterns of highly conductive pristine graphene on flexible substrates, Ind. Eng. Chem. Res. 53 (2014) 16777.
[28] E.B. Secor, M.C. Hersam, Emerging carbon and post-carbon nanomaterial inks for printed electronics, J. Phys. Chem. Lett. 6 (2015) 620.
[29] M. Michel, J.A. Desai, C. Biswas, A.B. Kaul, Optimization of fluid characteristics of 2D materials for inkjet printing, MRS Adv. 1 (2016) 2199.
[30] J.Y. Min, S. Yoon, J. Lee, S.J. Park, S.R. Kim, I. In, Submillimeter-scale graphene patterning through ink-jet printing of graphene oxide ink, Chem. Lett. 40 (2011) 54.
[31] M. Davidovich-Pinhas, S. Barbut, A. Marangoni, Physical structure and thermal behavior of ethylcellulose, Cellulose 21 (2014) 3243.
[32] A.G. Pineda, A. Hechenleitner, Characterization of ethylcellulose films containing natural polysaccharides by thermal analysis and FTIR spectroscopy, Acta Farm. Bonaer. 23 (2004) 53.
[33] M.K. Shahzad, M. Ubaid, M. Raza, G. Murtaza, The formulation of flurbiprofen loaded microspheres using hydroxypropylmethycellulose and ethylcellulose, Adv. Clin. Exp. Med. 22 (2012) 177.
[34] D.J. Finn, M. Lotya, J.N. Coleman, Inkjet printing of silver nanowire networks, ACS Appl. Mater. Interfaces 7 (2015) 9254.